



Controls governing the spatial distribution of sediment arsenic concentrations and solid-phase speciation in a lake impacted by legacy mining pollution

Christopher E. Schuh^{a,*}, Heather E. Jamieson^a, Michael J. Palmer^{b,1}, Alan J. Martin^c, Jules M. Blais^d

^a Department of Geological Sciences and Geological Engineering, Queen's University, Miller Hall, Kingston, ON K7L 3N6, Canada

^b NWT Cumulative Impact Monitoring Program, Government of the Northwest Territories, Yellowknife, NT X1A 2R3, Canada

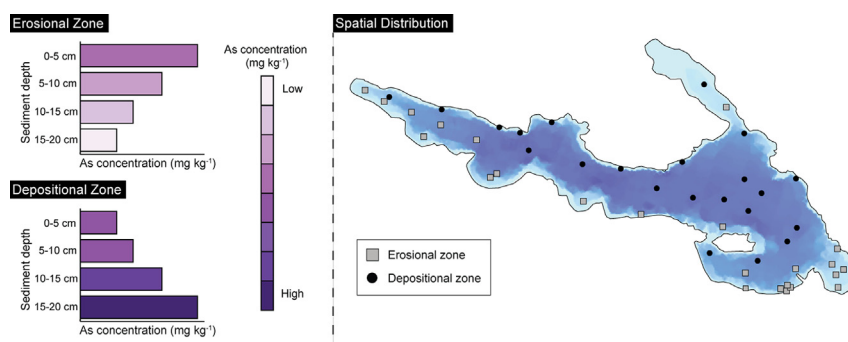
^c Lorax Environmental Services Limited, Vancouver, BC V6J 3H9, Canada

^d Department of Biology, University of Ottawa, Ottawa, ON K1N 6N5, Canada

HIGHLIGHTS

- Controls on the spatial distribution of As in mining-impacted lake sediments were investigated.
- Sediment cores and profiles of dissolved As in porewaters and bottom waters were collected.
- Sediment As concentrations, solid-phase speciation, and diffusive fluxes vary spatially.
- Spatial variability results from sediment focusing and its potential influence on As diagenesis.

GRAPHICAL ABSTRACT



ARTICLE INFO

Article history:

Received 29 August 2018

Received in revised form 30 October 2018

Accepted 5 November 2018

Available online 06 November 2018

Editor: F.M. Tack

Keywords:

Giant Mine

Arsenic trioxide

Ore roasting

Sediment focusing

Diagenesis

ABSTRACT

Forty-seven sediment cores were collected as part of a spatial survey of Long Lake, Yellowknife, NWT, Canada to elucidate the physical and geochemical controls on the distribution of arsenic (As) in sediments impacted by the aerial deposition of arsenic trioxide (As₂O₃) from ore roasting at legacy gold mines. High-resolution profiles of dissolved As in bottom water and porewater were also collected to determine As remobilization and diffusion rates across the sediment-water interface. Arsenic concentrations in Long Lake sediments ranged from 2.2 to 3420 mg kg⁻¹ (dry weight). Two distinct types of sediment As concentration profiles were identified and are interpreted to represent erosional and depositional areas. Water depth is the best predictor of As concentration in the top 5 cm of sediments due to the inferred focusing of fine-grained As₂O₃ into deeper water. At greater sediment depths, iron (Fe) concentration, as a likely indicator of As, Fe, and sulphur (S) co-diagenesis, was the best predictor of As concentration. The sediments are a source of dissolved As to surface waters through diffusion-controlled release to bottom water. Arsenic concentrations, solid-phase speciation, and diffusive efflux varied laterally across the lake bottom and with sediment depth due to the interplay between sediment-focusing processes and redox reactions, which has implications for human health and ecological risk assessments.

© 2018 Elsevier B.V. All rights reserved.

* Corresponding author.

E-mail address: c.schuh@queensu.ca (C.E. Schuh).

¹ Current address: Department of Geography and Environmental Studies, Carleton University, Ottawa, ON, K1S 5B6, Canada.

1. Introduction

Arsenic (As) is a naturally occurring metalloid that can cause toxic effects in humans and other organisms (e.g., Bissen and Frimmel, 2003). Anthropogenic activities can mobilize As into the environment through mining and ore processing, fossil-fuel combustion, and through the use of pesticides, herbicides, and wood preservatives that contain As (Bowell et al., 2014). Arsenic contamination from the mining and processing of orogenic gold deposits is a global issue due to the common occurrence of As-bearing sulphides in association with these deposits (Groves et al., 1998; Craw and Howell, 2014). The processing of arsenical ores can increase the rate at which As is released into the environment but can also induce mineralogical changes that influence As mobility, bioaccessibility, and toxicity (Smedley and Kinniburgh, 2002; Walker et al., 2015). For example, ore roasting is an oxidative pretreatment step that is used to improve gold recovery from refractory arsenopyrite (FeAsS) ores by roasting in the presence of an oxidizing gas, which produces a porous iron (Fe) oxide calcine from which gold can be more easily extracted by cyanidation (Marsden and House, 2006). Arsenic trioxide (As₂O₃) is produced as a byproduct of the roasting process and is considered the most bioaccessible As-hosting solid compound in human bodily fluids, especially in comparison to naturally occurring arsenopyrite, which is less soluble and bioaccessible (Plumlee and Morman, 2011). The atmospheric release of bioaccessible As₂O₃ from ore-roasting operations can lead to its accumulation in nearby aquatic environments. In this regard, lake sediments contaminated by legacy As pollution may represent a long-term source of As to overlying waters and aquatic ecosystems.

Stack emissions from the roasting of As-bearing ores at legacy gold mines near Yellowknife, NWT, Canada, have resulted in As concentrations in regional lake sediments that are elevated relative to Canadian guidelines (Galloway et al., 2018; Schuh et al., 2018; Van Den Berghe et al., 2018). Ore roasting at the Giant Mine occurred from 1949 to 1999 and was conducted at 500 °C to convert gold-bearing arsenopyrite to gold-bearing Fe oxides, from which gold could be extracted using cyanide leaching (Walker et al., 2015). By-products of the roasting process included As₂O₃, which, in the early years of operations, was released directly to the atmosphere. The As₂O₃ produced at Giant Mine also contains antimony (Sb) due to the presence of Sb-bearing minerals in the roasted ores (Riveros et al., 2000). Approximately 20,000 t of As₂O₃ were released to the atmosphere during operations, the majority of which was released before the construction of a baghouse facility to capture As₂O₃ dust in 1958 (Wrye, 2008). The roasting of arsenical gold ores also occurred in the early years of mining at the nearby Con Mine (1938–2003), although Giant Mine is considered the largest anthropogenic source of As in the region (Mackenzie Valley Review Board, 2013).

Human Health (HHRA) and Ecological Risk Assessments (ERA) were recently conducted by Canada North Environmental Services (2018) to quantify the risk of exposure to As for humans and other organisms on the Giant Mine site and in the Yellowknife area. Multiple contaminant-exposure pathways were considered including air, household dust, soil, sediments, water, and country foods. For sediments and lake water, potential routes of exposure considered included dermal contact and ingestion. Wading and swimming in contaminated sediments and lake water were shown to contribute to the incremental intake of As, though estimated risks were classified as very low (i.e., the incremental lifetime cancer risk level was between 1:10,000 and 1:100,000) (Health Canada, 2010). The ERA found high levels of As in sediments and lake water to adversely affect aquatic biota in water bodies on and adjacent to the Giant Mine property, however, the potential for As to cause adverse ecological effects in lakes beyond mine-property boundaries was not assessed.

The biogeochemical cycling of As in lake sediments is closely associated with the cycling of Fe, manganese (Mn), sulphur (S), and organic carbon (OC) (Couture et al., 2010). In lakes with oxygenated bottom

waters, authigenic Fe- and Mn-oxyhydroxides accumulate at the sediment-water interface and can sequester dissolved As through adsorption and co-precipitation processes. Microbes that oxidize OC as an energy source, which is supplied to interfacial sediments through the settling of organic material, first use available oxygen (O₂) as an oxidant but, as conditions become progressively suboxic during burial, Fe- and Mn-oxyhydroxides reductively dissolve and may release associated As to sediment porewaters (Boudreau, 1999; Martin and Pedersen, 2002; Campbell et al., 2008). The resulting concentration gradient causes dissolved As to diffuse upward toward the sediment-water interface where it can be re-sequestered by authigenic metal oxyhydroxides or released into the overlying water column (Boudreau, 1999; Martin and Pedersen, 2002). The potential for the release of dissolved As into the water column depends on sediment redox conditions, which are, in turn, governed by the accumulation rate of OC. Where the position of the ferric Fe (Fe³⁺) redoxcline is deep relative to the sediment-water interface, a significant proportion of the upward diffusive flux can be expected to be sequestered by Fe- and Mn-oxyhydroxides in oxic interfacial horizons. In contrast, where the depth of the Fe³⁺ redoxcline is shallow, a greater proportion of the upward diffusing As can be expected to migrate into the water column (Martin and Pedersen, 2002; Andrade et al., 2010; Moriarty et al., 2014; Sprague and Vermaire, 2018). Dissolved As may also diffuse downward where it can be removed from solution through the precipitation of As-bearing pyrite (FeS₂) or discrete As-sulphides such as realgar (As₄S₄) and orpiment (As₂S₃) (Bostick and Fendorf, 2003; O'Day et al., 2004; Lowers et al., 2007; Schuh et al., 2018). Therefore, the vertical distribution of As in sediments can be strongly influenced by redox conditions and the associated early diagenesis of Fe, Mn, and S. The depth distribution of As in lake sediments in the Yellowknife area, however, is the result of these processes and the historical deposition of As from ore roasting (Schuh et al., 2018; Van Den Berghe et al., 2018). Arsenic enrichment at depth in the sediment column is a product of the historical aerial deposition of stack emissions from former ore-roasting operations in the region. In these horizons of peak As concentration, As is predominantly hosted in As₂O₃ or secondary As-bearing sulphides that precipitate following its partial dissolution (Schuh et al., 2018; Van Den Berghe et al., 2018). Arsenic enrichments at the sediment-water interface are primarily associated with authigenic Fe-oxyhydroxide (Schuh et al., 2018). These secondary phases (As-bearing sulphides and Fe-oxyhydroxide) are less bioaccessible than As₂O₃ (Plumlee and Morman, 2011).

Spatially, the distribution of As in lake sediments may also be influenced by physical processes that erode and redistribute fine-grained material from shallow-water areas to zones of deposition in deeper parts of the lake basin (Blais and Kalff, 1995). The areal extent of these zones is dependent on lake morphometric variables including water depth and basin slope (Håkanson, 1977). Wind-driven mixing processes that resuspend and transport sediments are strongest at the lake surface and lose strength with increasing water depth (Mackay et al., 2012). Sediment resuspension caused by wind-generated waves is specifically dependent on water depth and fetch. In areas of lakes with large fetch to depth ratios, the energy of wave-induced turbulence is sufficient to reach the sediment surface and cause resuspension (Hamilton and Mitchell, 1997). Sediment resuspension and focusing processes are also strongly driven by slumping, sliding, and turbidity currents, which are often caused by gravity-driven bed slope failures (Håkanson and Jansson, 2011). In water bodies that are ice-covered for much of the year, such as lakes in the Yellowknife area, ice scouring of the sediment surface may also contribute to nearshore erosion and sediment resuspension (Héquette et al., 1999).

Studies that use sediment cores as historical records of the atmospheric deposition of As and other contaminants typically rely on a single sediment core collected from the deepest and most central part of a lake basin (Z_{\max}) because sediments from this area are thought to be most representative of lake-wide processes (Engstrom and Rose,

2013). Sediment deposition across a lake basin, however, varies laterally because of sediment focusing, and therefore chemical profiles in sediment cores from Z_{\max} may not be representative of whole-lake accumulation trends. Sediment redistribution processes also have the potential to indirectly influence the depositional patterns and post-depositional mobility of As by focusing Fe, S, OC, and other elements involved in its redox cycling. To account for spatial variability in lake sediment properties, other studies have employed a multi-station coring approach (Rippey et al., 2008; Engstrom and Rose, 2013; Lin et al., 2018).

The objectives of this research were to describe the spatial variation in sediment As concentrations and solid-phase speciation, both laterally across the lake basin and with depth through the sediment profile, in a lake impacted by the historical aerial deposition of As, and to better understand the physical and geochemical processes governing this variation. An additional goal was to compare rates of As remobilization and release into the overlying water column at two locations to highlight factors that may drive the spatial variability of As fluxes. In addition to

broadening our understanding of As behaviour in contaminated lakes, the results presented here are expected to provide valuable information to support human health and ecological risk assessments in areas affected by the deposition of As from legacy mining operations. Specifically, defining the controls governing the abundance and speciation of As in lake sediments allows for the delineation of lake zones where increased exposure to high sediment As concentrations and more bioaccessible As-hosting solid phases is most likely.

2. Methods

2.1. Study site

Long Lake is located approximately 5 km southwest and 5 km northwest of the former roasters at Giant Mine and Con Mine, respectively ($62^{\circ} 28' 18.12''$ N, $114^{\circ} 25' 39.72''$ W) (Fig. 1a,b). Bathymetric mapping in 2016 (Fig. 1c) indicated that the lake has a surface area of 1.16 km^2 , a

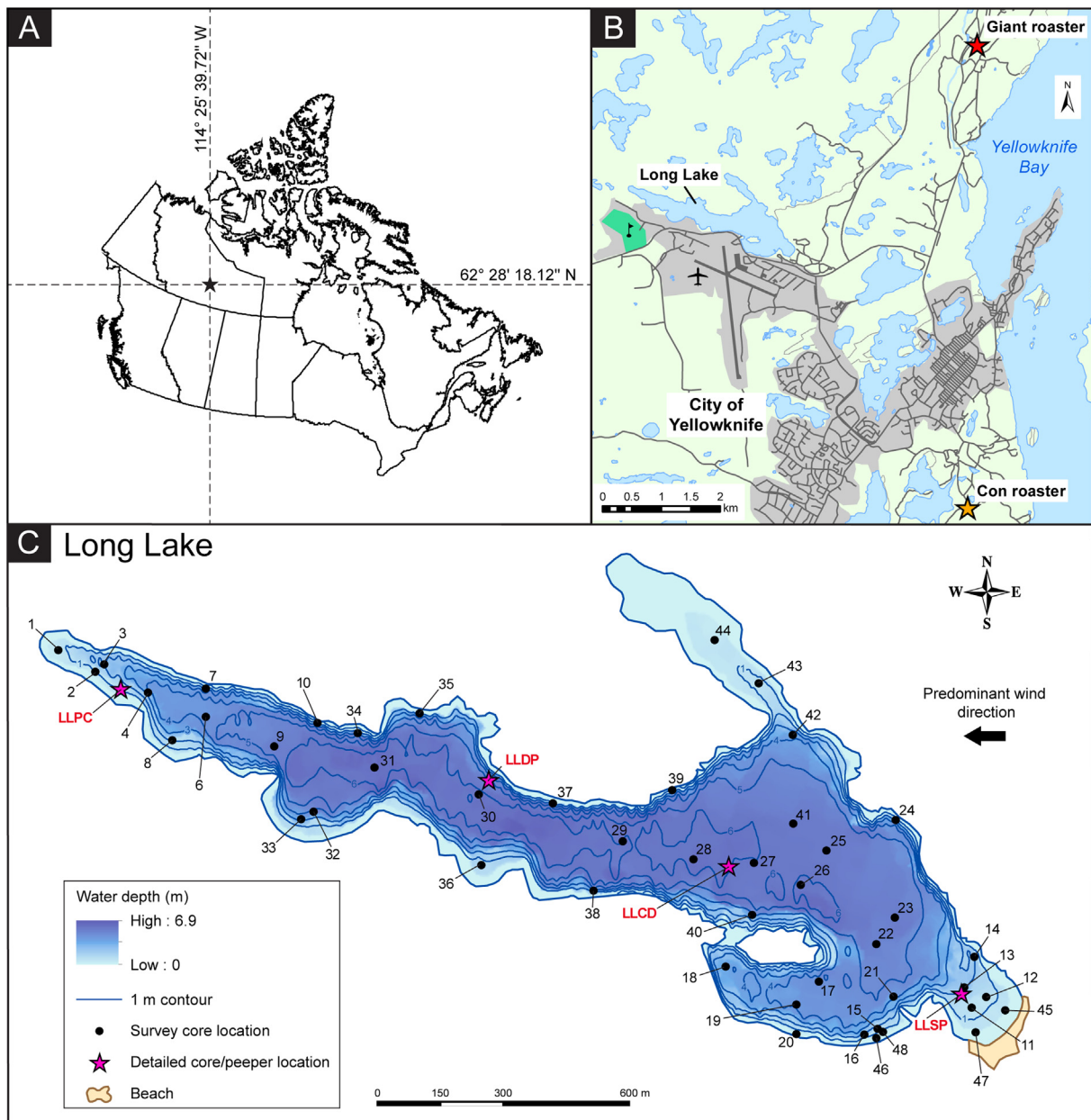


Fig. 1. (a) Location of study area within Canada. (b) Location of Long Lake relative to the City of Yellowknife and the former roasters at Giant Mine and Con Mine. (c) 2016 bathymetric map of Long Lake showing sample locations. (For interpretation of the references to colour in this figure legend, the reader is referred to the web version of this article.)

total volume of $4.26 \times 10^6 \text{ m}^3$, an average depth of 3.7 m, and a maximum depth (Z_{max}) of 6.9 m. The northern shore of the lake is characterized by exposed granitic and mafic-volcanic outcrops. Water depths along this shore increase abruptly, as demonstrated by the steep contours in Fig. 1c. Comparatively, water depths along the southern shore, which is adjacent to road infrastructure, increase more gradually. Long Lake is not connected to any inflow or outflow streams. The main inputs of water to the basin are precipitation and terrestrial runoff, and outputs are likely limited to surface evaporation and ephemeral seepage. The lake is well-mixed and ice-free from approximately June to October, and ice-covered ($\sim 0.6\text{--}0.8$ m thickness) the rest of the year. Winds over the water surface generally blow from east to west based on climate data measured over a 30-year period (1970–2010) at the nearby Yellowknife Airport (Environment Canada, 2017) (Fig. 1b). The Yellowknife Golf Club is located near the southern shore (Fig. 1b) and features sand fairways. The lake is used for recreation by the local population and features a constructed sand beach, boat launch, and campground at the southeastern shore (Fig. 1c). Sixteen sediment grab samples were collected near the beach and boat launch area in 2016 as part of the recent HHRA (Canada North Environmental Services, 2018). Sediment As concentrations ranged from 7 to 100 mg kg^{-1} (dry weight). The bioavailability of these samples was assumed to be 45% based on the average bioavailability measured in five samples. The HHRA concluded that dermal contact with these sediments may contribute to the incremental intake of As, though estimated risks are very low according to Health Canada (2010) guidelines. Arsenic exposure to aquatic organisms in Long Lake was not evaluated as part of the recent ERA (Canada North Environmental Services, 2018). The concentration of dissolved As in surface water measured in 2014 was $40 \text{ } \mu\text{g L}^{-1}$ (Palmer et al., 2015).

2.2. Sample collection

Forty-seven sediment cores were collected from Long Lake in July 2016 as part of a spatial survey to assess the horizontal and vertical distribution of As within sediments (Fig. 1c). Sediment cores were collected by motor boat using a 7.5 cm internal diameter gravity corer (Glew, 1989) from sample locations chosen to maximize spatial coverage of the basin. A higher density of samples was collected near the beach and boat launch area (Fig. 1c) which is frequented by swimmers. Sediment cores were extruded on shore and the top 20 cm of each core were sectioned in 5 cm intervals (0–5 cm, 5–10 cm, 10–15 cm, and 15–20 cm). The penetration depth of the sediment corer was variable, and only 22 cores penetrated to a sediment depth greater than or equal to 20 cm. Two additional cores (30 cm penetration depth) were collected at sites LLSP and LLDP (Fig. 1c) and sectioned at higher resolution. These cores were extruded in the laboratory in a nitrogen (N_2)-purged glove bag to preserve solid-phase As speciation; the top 30 cm of each core were sectioned into 1 cm (0–20 cm) and 2 cm (20–30 cm) intervals. Sediment samples were extruded into Whirl-Pak® bags, homogenized, and refrigerated for approximately 1–2 weeks prior to analyses.

In July 2016, high-resolution dialysis arrays (peepers) with $0.45 \text{ } \mu\text{m}$ filter membranes and sample cells spaced 0.77 cm centre-to-centre, were installed back-to-back by scuba-diver insertion at site LLSP (Fig. 1c). The peepers were installed with cells above and below the sediment-water interface to capture concentrations of dissolved solutes in porewaters and bottom waters. The preparation of peepers prior to field deployment was described previously (Schuh et al., 2018). After 14 days of equilibration with porewaters and bottom waters, water samples were extracted from peeper cells in a N_2 -purged glovebox. Samples to be analyzed for trace metal(loid) concentrations were preserved with 8 M HNO_3 , and samples for aqueous inorganic As speciation were preserved with 0.25 M ethylenediaminetetraacetic acid (EDTA) and glacial acetic acid (Bednar et al., 2002). Samples were immediately refrigerated and held for approximately one week prior to analysis.

2.3. Sediment and water analyses

Metal(loid) concentrations in sediment (30 analytes) and water (25 analytes) samples were determined using inductively coupled plasma optical emission spectroscopy (ICP-OES) and inductively coupled plasma mass spectrometry (ICP-MS). ICP-OES was used for the determination of element concentrations in sediments, but ICP-MS was used to achieve lower detection limits for some elements, including As and Sb. ICP-MS was used exclusively for water analyses. Prior to analysis, sediment samples were digested in accordance with USEPA Method 200.2 (Martin et al., 1994a). The determination of metal and trace element concentrations by ICP-OES and ICP-MS followed USEPA Methods 200.7 (Martin et al., 1994b) and 200.8 (Creed et al., 1994), respectively. All sediment element concentrations reported in this paper are dry-weight concentrations. The relative proportions of dissolved arsenate (As^{5+}) and arsenite (As^{3+}) in water samples were determined using hydride generation atomic fluorescence spectrometry (HG-AFS). Total organic carbon (TOC) concentrations in survey sediment samples were determined by dry combustion using a Leco CNS-2000 Analyzer. Due to insufficient sample volumes, only selected sediment samples were texturally classified based on their sand, silt, and clay content (Shepard, 1954). Grain size in these samples was determined using Hydrometer Method 55.3 in Carter and Gregorich (2007).

The quality-control guidelines outlined in USEPA Methods 200.7 (Martin et al., 1994b) and 200.8 (Creed et al., 1994) were followed to ensure that data were of acceptable quality for use. For sediments, analytical precision was evaluated by analyzing duplicate samples (six sets); analytical accuracy was assessed by analyzing certified reference material MESS-3 ($n = 4$) and laboratory control samples ($n = 2$). Duplicate analyses yielded relative percent difference values below 20% for all analytes including As, Sb, Fe, Mn, S, TOC, and grain size. In certified reference materials and laboratory control samples, recovery values for all analytes were within an acceptable range (70–130%). Laboratory blanks were also analyzed at a minimum of every 20 samples to evaluate potential sources of contamination; all analyte concentrations were below method detection limits in all blanks. Additionally, instrument calibration checks were performed at the beginning of analyses and throughout analyses at a minimum of every 20 samples. The same quality-control guidelines were followed for the analyses of porewater and bottom water samples, however, the small sample volumes ($<4 \text{ mL}$) obtained from peeper cells precluded the analysis of duplicates.

2.4. Solid-phase arsenic speciation

The identification of As-hosting solid phases in selected sediment samples from high-resolution cores LLSP and LLDP (Fig. 1c) was accomplished using scanning electron microscopy (SEM)-based automated mineralogy (Schuh et al., 2018; Van Den Bergh et al., 2018). Sediment-depth intervals associated with high As concentrations and sediments from the bottom of each core were subsampled and dried in a N_2 -purged glove bag to preserve As-hosting solid phases. Polished sections were then made by mounting dried sediment in epoxy on glass slides and polishing in kerosene to $30 \text{ } \mu\text{m}$ thickness. From the LLSP core, polished sections were prepared for the following depth intervals: 0–1 cm (sample LLSP-01), 5–6 cm (sample LLSP-06), and 26–28 cm (sample LLSP-24). Polished sections were prepared for the following sediment horizons from the LLDP core: 0–1 cm (sample LLDP-01), 5–6 cm (sample LLDP-09), and 28–30 cm (sample LLDP-25).

Automated mineralogy was performed using a FEI™ Quanta 650 Field Emission Gun Environmental SEM and Mineral Liberation Analyzer (MLA) software. Operating conditions, backscatter electron image standardization and resolution, X-ray acquisition modes, the mineral reference library used for phase classification, and the calculations used to quantify the relative contribution of each As-hosting phase, by mass, to total As concentrations, are the same as in Schuh et al. (2018). The concentrations of As associated with Fe-

oxyhydroxide and framboidal pyrite used in the calculations were 3 wt% and 0.2 wt%, respectively, based on electron microprobe measurements by Schuh et al. (2018).

2.5. Statistical analyses

Statistical analyses were performed to investigate the relationships between sediment As concentrations and other relevant variables. Using the Anderson–Darling test, the concentrations of As and other associated geochemical variables (Sb, Fe, Mn, S, and TOC) in all sediment depth intervals, as well as water depth, were found to be not normally distributed. Spearman's rank order correlation analysis was therefore used to examine the relationships between variables (O'Brien, 2007). The relationships between As and variables anticipated to be directly involved in controlling As concentrations in sediments (Fe, S, and water depth) were further explored using multiple linear regression. Prior to performing the regression analyses, continuous predictor variables were converted to units of standard deviation from the mean (i.e., z values) to allow for direct comparisons between regression coefficients (Harris and Jarvis, 2010). Method detection limits were used for values that were reported below the method detection limit. All tests were performed at a 95% confidence interval ($\alpha = 0.05$) using Minitab 18 (2017).

2.6. Arsenic flux calculations

Concentration gradients of dissolved As in porewaters and bottom waters collected at sites LLSP (this study) and LLPC (Schuh et al., 2018) (Fig. 1c) were calculated following methods outlined in Martin and Pedersen (2002) to estimate (1) As remobilization rates in sediments, and (2) rates of As diffusion into the overlying water column. At each site, rates of As remobilization were determined using linear concentration gradients above the porewater maximum, while efflux rates (i.e., diffusion across the benthic boundary) were calculated using assumed linear concentration gradients from approximately 1 cm depth to the sediment–water interface. Arsenic concentration gradients across the sediment–water interface are typically non-linear due to the removal of As from solution via sorption with Fe- and Mn-oxyhydroxides, which likely results in an overestimation of the magnitude of the concentration gradient. Rates of diffusive transport, J_z ($\mu\text{g cm}^{-2} \text{ year}^{-1}$), were calculated using Fick's first law:

$$J_z = -\frac{D_j^0}{F} \phi \frac{dc}{dz} \quad (1)$$

where D_j^0 is the coefficient of diffusion ($\text{cm}^2 \text{ s}^{-1}$), F is the formation factor, ϕ is sediment porosity, and dc/dz is the concentration gradient. Values of D_j^0 were calculated using a temperature of 20 °C, known values for As^{5+} (H_2AsO_4^-) and As^{3+} (H_3AsO_3) at 25 °C (Tanaka et al., 2013), and the Stokes–Einstein relation. The calculations were performed using diffusion coefficients for both As^{5+} and As^{3+} to explore how remobilization and efflux rates might vary laterally across the lake bottom with changing redox conditions and differing $\text{As}^{5+}/\text{As}^{3+}$ ratios in interfacial porewaters. The formation factor, F , accounts for the tortuous path taken by diffusing ions in a porous medium and was calculated from porosity using Archie's law (Ullman and Aller, 1982). Negative flux values imply that the direction of diffusive transport is upward (Martin and Pedersen, 2002). Input values used to calculate diffusion rates are summarized in Supplementary Data Table S1.

Relative rates of As burial in sediments were estimated by multiplying low and high sediment As concentrations (100 and 3000 mg kg^{-1} , respectively) by an assumed sedimentation rate of 0.1 $\text{g cm}^{-2} \text{ year}^{-1}$. The sedimentation rate was determined using inventories of ^{210}Pb in core LLCD (Schuh et al., 2018) (Fig. 1c) and the constant rate of supply model (Appleby, 2001).

3. Results

3.1. Sediment arsenic concentrations

Arsenic concentrations in Long Lake sediments varied horizontally across the lake bottom and with depth in the sediment column (Fig. 2; Table S2). In the upper 5 cm of sediments, As concentrations ranged from 4.6 to 1180 mg kg^{-1} (median 593 mg kg^{-1} , $n = 47$). In sediments 5–10 cm below the sediment surface, As concentrations exhibited greater variability, ranging from 2.4 to 1800 mg kg^{-1} (median 679 mg kg^{-1} , $n = 45$). Arsenic concentrations in the 10–15 cm sediment depth interval varied by three orders of magnitude, ranging from 2.2 to 2330 mg kg^{-1} (median 425 mg kg^{-1} , $n = 33$). Arsenic concentrations within the 15–20 cm interval were the most variable and ranged from 3.2 to 3420 mg kg^{-1} (median 259 mg kg^{-1} , $n = 22$). Summary results for other relevant sediment analytes (Sb, Fe, Mn, S, TOC, and grain size) are provided in Tables S3–S8.

Two distinct categories of As concentration profiles were identified in Long Lake sediments (Fig. 2). In the first type of profile, henceforth referred to as *erosional-zone* (Type E) profiles, As concentrations were highest in surficial (0–5 cm) sediments and decreased with depth (e.g., cores 6 and 22). In comparison, *depositional-zone* (Type D) profiles were those in which the highest As concentrations occurred at sediment depths >5 cm, and generally occurred in sediments 5–15 cm below the sediment surface (e.g., cores 27 and 28).

Arsenic concentration profiles in high-resolution sediment cores LLSP and LLDP (Fig. 2) exhibited characteristics of Type D and Type E profiles, respectively. In the LLSP core (Fig. 3; Table S9), which was collected at 2 m water depth, the maximum As concentration of 860 mg kg^{-1} (sample LLSP-06) occurred in sediments approximately 5–6 cm below the sediment surface, which is characteristic of Type D profiles. However, sub-sampling at higher resolution revealed the existence of a second As peak of 520 mg kg^{-1} (sample LLSP-01) at the sediment–water interface. Below a sediment depth of approximately 10 cm, As concentrations decreased to relatively low levels that may represent pre-mining conditions (Galloway et al., 2015). In comparison, only one sediment As maximum of 1300 mg kg^{-1} (sample LLDP-01), occurring at the sediment surface, was present in the As concentration profile in the LLDP core (Fig. 3; Table S10), which was collected at 5.5 m water depth. Arsenic concentrations progressively decreased to a sediment depth of approximately 20 cm before reaching assumed background levels. Sediment concentrations of Sb, Fe, Mn, and S in cores LLSP and LLDP are presented in Tables S9 and S10.

3.2. Arsenic-hosting solid phases

The predominant As-hosting solid phases in cores LLSP and LLDP were identified using SEM-based automated mineralogy. Roaster-derived As_2O_3 , with trace Sb and occurring as isolated grains, was identified as a host of As in sediments from both high-resolution cores. Authigenic As-hosting phases were also identified and included Fe-oxyhydroxide, realgar, and framboidal pyrite, which are interpreted to form in situ from the partial dissolution of As_2O_3 (Schuh et al., 2018; Van Den Berghe et al., 2018). Authigenic Fe-oxyhydroxide and pyrite were distinguished from their detrital counterparts based on texture (Schuh et al., 2018). The mass distribution of As-hosting phases in selected samples is shown in Fig. 3.

In core LLSP, As-bearing Fe-oxyhydroxide comprised approximately 83% of the total As concentration in interfacial sediments (sample LLSP-01) (Fig. 3). Three As_2O_3 particles were identified in this interval and accounted for approximately 5% of the total As inventory; the remaining 12% was associated with framboidal pyrite. In sediments associated with the As maximum at 5–6 cm depth (sample LLSP-06), particles of As_2O_3 contributed approximately 34% to the total As concentration. The As-bearing sulphides realgar and framboidal pyrite accounted for approximately 58% and 7% of the total As concentration, respectively.

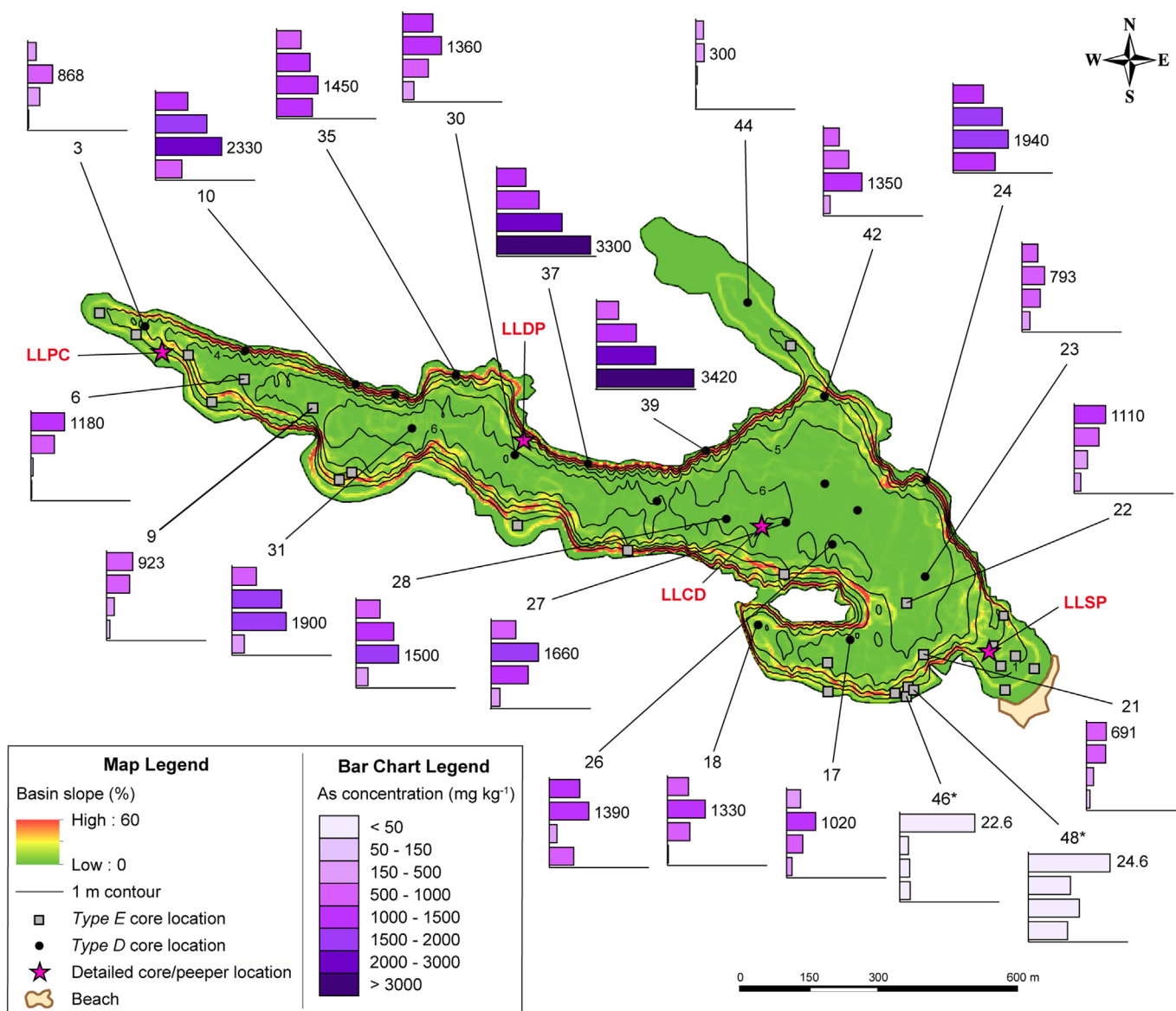


Fig. 2. 2016 bathymetric map of Long Lake showing the spatial distribution of As concentration profiles in full 20 cm sediment cores ($n = 22$), shown as bar charts, relative to changes in basin slope. Grey squares and black dots denote *Type E* and *Type D* cores, respectively. For bar charts, sediment depth (cm) is plotted on the y-axis and each bar represents one of the sediment depth intervals subsampled (0–5 cm, 5–10 cm, 10–15 cm, and 15–20 cm). Arsenic concentrations (mg kg^{-1}) are plotted on the x-axis (0–3500 mg kg^{-1}) and maxima are labelled. Profiles with an asterisk are plotted on an x-axis with 0–30 mg kg^{-1} scale. (For interpretation of the references to colour in this figure legend, the reader is referred to the web version of this article.)

Rare arsenopyrite grains were also identified in sample LLSP-06, but their contribution to the total As concentration was low (<1%). Virtually 100% of the sediment As concentration in sample LLSP-24 was associated with framboidal pyrite.

In comparison, the near surface As maximum in the LLDP core (sample LLDP-01) comprised As_2O_3 (14%), Fe-oxyhydroxide (43%), realgar (42%), and framboidal pyrite (1%) (Fig. 3). At approximately 8.5 cm depth (sample LLDP-09), realgar (69%) and As-bearing pyrite (21%) constituted approximately 90% of the total As concentration, and rare As_2O_3 particles accounted for the remaining 10%. Like in the LLSP core, trace concentrations of As associated with framboidal pyrite effectively comprised 100% of the total As concentration in bottom-core sediments (sample LLDP-25).

3.3. Relationships between variables

Spearman's rank order correlation analysis indicated that As was positively and significantly ($p < 0.05$) correlated with Sb, Fe, Mn, S,

TOC, and water depth in all sediment depth intervals (Fig. 4). Arsenic was most strongly positively correlated ($\rho \geq 0.90$) with Sb at all depths, with strong positive correlations also consistently observed with Fe and Mn. The strength of the As relationships to other variables changed with sediment depth. The association between As and water depth was highest in near-surface sediments and decreased with sediment depth. Conversely, the strength of the relationship between As and S was lowest in surficial sediments and increased to a depth of 15 cm, but decreased in the 15–20 cm interval. Similarly, As and TOC were most positively correlated in the top 10 cm of sediments, with the strength of the relationship decreasing at depth. Sulphur and TOC were also most positively correlated in the top 10 cm of sediments, whereas the relationship between Fe and TOC was comparatively weak at all sediment depths. The concentrations of Sb, Fe, Mn, S, and TOC were strongly and significantly correlated with water depth in all sediment depth intervals (Fig. 4).

Stepwise multiple linear regression was used to assess the relative importance of Fe concentration, S concentration, and water depth,

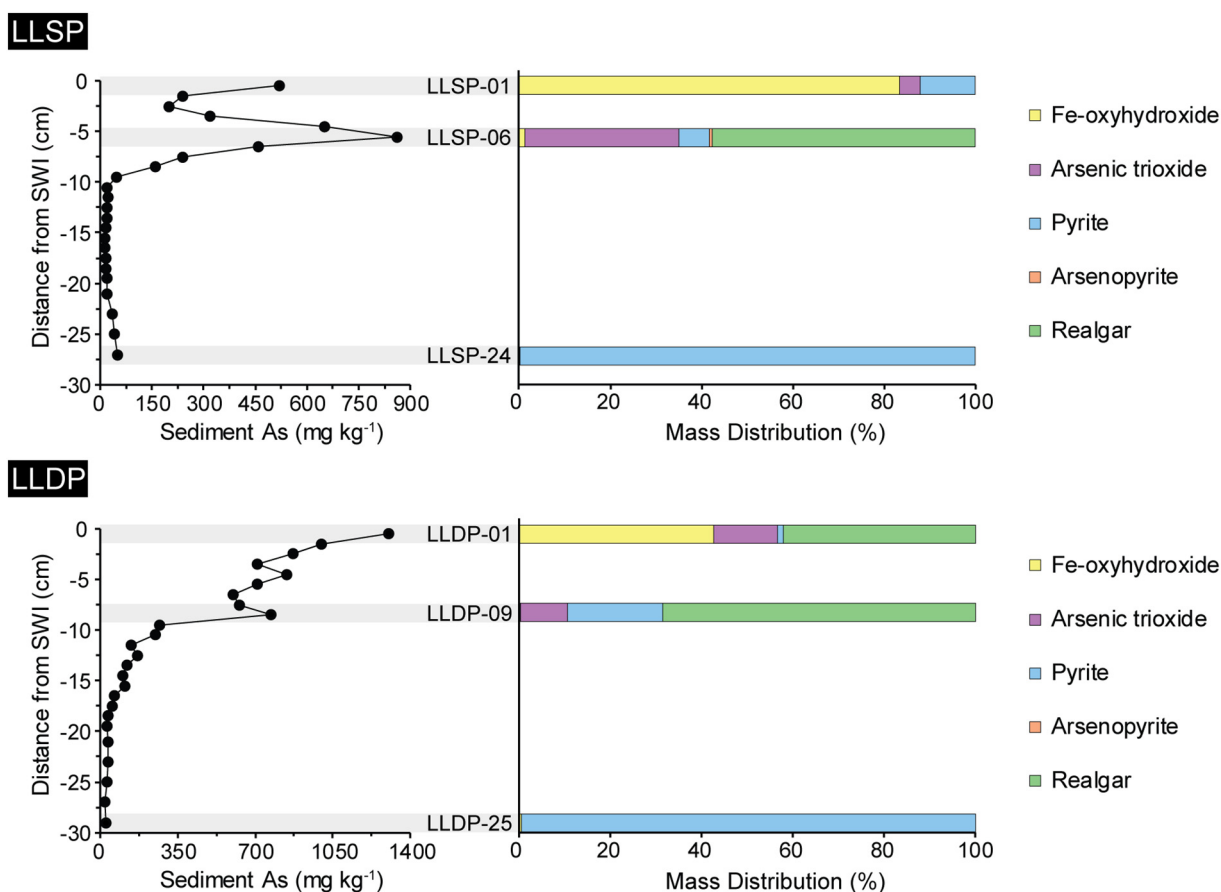


Fig. 3. Arsenic concentration profiles in high-resolution sediment cores LLSP and LLDP, which exhibit characteristics of Type D and Type E profiles, respectively. Bar charts show the relative contribution of each As-hosting solid phase, by mass, to total As concentrations in selected sediment intervals. SWI = sediment-water interface. (For interpretation of the references to colour in this figure legend, the reader is referred to the web version of this article.)

alone and in combination, as predictors of sediment As concentration in all sediment depth intervals (Table S11). In near-surface sediments, the strongest model was produced using only Fe and water depth as predictors of As abundance (adjusted $R^2 = 0.86$, $p < 0.001$). The standardized regression coefficients (0.45 and 0.51 for Fe and water depth, respectively) indicated that water depth is a marginally better predictor of As concentration in surficial sediments than Fe concentration. In sediments 5–10 cm below the sediment surface, the strongest model included all three predictors (adjusted $R^2 = 0.79$, $p < 0.001$), although Fe and water depth were found to have a greater influence on As concentration than S as illustrated by standardized regression coefficients (0.38, 0.24, and 0.37 for Fe, S, and water depth, respectively). In the 10–15 cm sediment depth interval, water depth was no longer a significant predictor of As concentration, as the best-fitting model included only Fe and S as predictive variables (adjusted $R^2 = 0.64$, $p < 0.001$). At this depth, comparison of standardized regression coefficients (0.51 and 0.37 for Fe and S, respectively) suggested that Fe concentration has a greater effect on As concentration as compared to S. In sediments 15–20 cm below the sediment-water interface, the strongest model was again produced using only Fe and S as predictors (adjusted $R^2 = 0.83$, $p < 0.001$), and Fe was found to have approximately two times greater effect on As concentration than S through comparison of standardized regression coefficients (1.48 and -0.75 for Fe and S, respectively). The regression coefficient for S was negative, indicating that an increase in S concentration within this interval is associated with a decrease in As concentration. Variance inflation factors (VIFs) for all depth intervals ranged from 2 to 4, indicating moderate correlation between predictors but not so much as to result in poor estimation of regression coefficients (O'Brien, 2007).

3.4. Arsenic fluxes

Concentration profiles of dissolved solutes across the sediment-water interface at site LLSP are shown in Fig. 5. From 1.5 cm above the sediment-water interface ($17 \mu\text{g L}^{-1}$) to a sediment depth of approximately 1.5 cm ($32 \mu\text{g L}^{-1}$), dissolved As concentrations increased non-linearly (i.e., concave upward) and remained fairly constant (Fig. 5a; Table S12). Below this interval, however, dissolved As concentrations increased more linearly with depth and reached a maximum concentration ($500 \mu\text{g L}^{-1}$) approximately 7 cm below the sediment-water interface, which is approximately 1 cm below the sediment maximum (Fig. 3). Porewater As concentrations decreased slightly with depth below the maximum, but remained high relative to concentrations in near-surface porewaters. Trends in the porewater profiles of Fe and Mn were similar to As (Fig. 5b; Table S12).

Across the sediment-water interface, As^{3+} was the dominant inorganic aqueous As species at site LLSP (Fig. 5a; Table S12). Approximately 1.5 cm above the benthic boundary, As^{3+} comprised approximately 78% of inorganic dissolved As species. The highest $\text{As}^{5+}/\text{As}^{3+}$ ratio occurred in porewaters 0.77 cm below the sediment surface, where As^{5+} and As^{3+} accounted for 40% and 60% of measured As species, respectively. Below a depth of 5 cm, the relative proportion of As^{3+} was consistently $>90\%$ (Fig. 5a; Table S12).

The rates of dissolved As remobilization toward the sediment-water interface at site LLSP were calculated as $-7 \mu\text{g cm}^{-2} \text{year}^{-1}$ for As^{5+} and $-9 \mu\text{g cm}^{-2} \text{year}^{-1}$ for As^{3+} using Fick's first law (Eq. (1)), the linear concentration gradient of dissolved As above the porewater maximum, and an estimated porosity of 0.6 (Manger, 1963) based on grain size measurements in sediments from nearby core 13 (Fig. 1c;

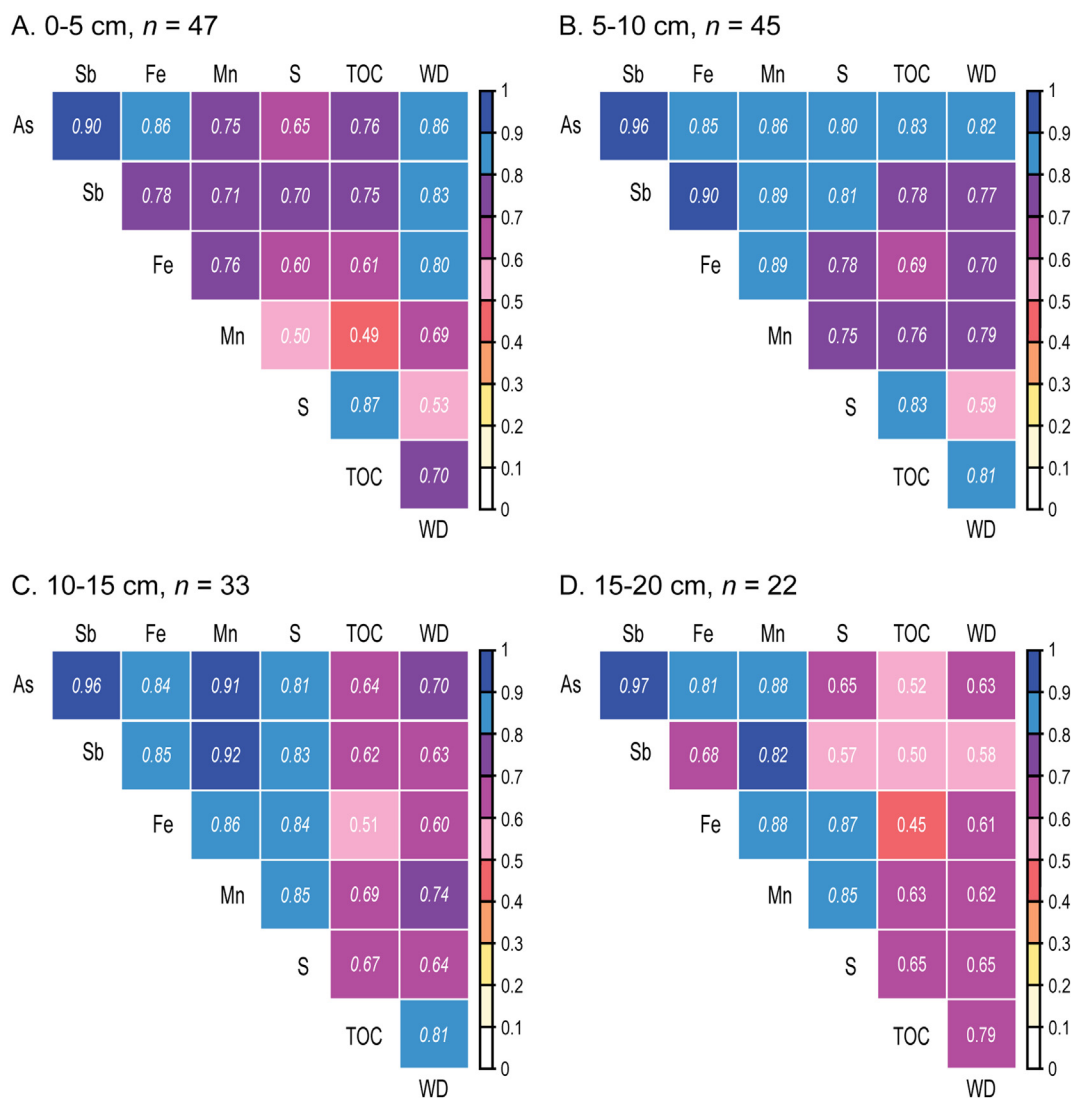


Fig. 4. Spearman's rank order correlation matrices for sediments from all four depth intervals (a-d). All Spearman's rho values are statistically significant ($p < 0.05$). Highly significant values ($p < 0.001$) are italicized. WD = water depth. (For interpretation of the references to colour in this figure legend, the reader is referred to the web version of this article.)

Table S8). Similarly, an assumed linear concentration gradient of dissolved As across the sediment-water interface was used to determine rates of As^{5+} and As^{3+} diffusion into the overlying water column, which were calculated as -0.4 and $-0.6 \mu\text{g cm}^{-2} \text{year}^{-1}$, respectively, indicating As release from the sediments into lake bottom waters.

The same calculations were repeated using the dissolved As concentration profile measured in sediments at site LLPC by Schuh et al. (2018) and an estimated porosity of 0.4 (Manger, 1963) based on grain size measurements from nearby core 2 (Fig. 1c; Table S8). At this site, which is located in relatively shallow water (0.7 m water depth), As^{5+} accounted for 95% of measured dissolved As species at the sediment-water interface (Schuh et al., 2018). Upward remobilization rates for As^{5+} and As^{3+} were calculated as -1 and $-2 \mu\text{g cm}^{-2} \text{year}^{-1}$, respectively. Rates of efflux across the sediment-water interface were calculated as $-0.2 \mu\text{g cm}^{-2} \text{year}^{-1}$ for As^{5+} and $-0.3 \mu\text{g cm}^{-2} \text{year}^{-1}$ for As^{3+} . The results of all diffusion calculations are summarized in Table S13. Relative rates of As deposition and burial were calculated as 10 and $300 \mu\text{g cm}^{-2} \text{year}^{-1}$ using low (100 mg kg^{-1}) and high (3000 mg kg^{-1}) sediment As concentrations, respectively, and an assumed sedimentation rate of $0.1 \text{ g cm}^{-2} \text{year}^{-1}$ (Schuh et al., 2018).

4. Discussion

4.1. Physical controls on the spatial distribution of arsenic in sediments

The results of Spearman's rank order correlation analysis indicated that solid-phase concentrations of both As and Sb, which are strongly correlated due to the presence of Sb in the As_2O_3 produced by roasting (Riveros et al., 2000; Schuh et al., 2018), are positively and significantly correlated ($\rho = 0.58-0.86$, $p < 0.05$) with water depth in all sediment depth intervals (Fig. 4). This suggests that sediment concentrations of As_2O_3 particles, the majority of which were aerally deposited, are largely controlled by changes in water depth. Such observations are consistent with the fine particle sizes of aerally-deposited As_2O_3 ($\sim 2-30 \mu\text{m}$ diameter) (Schuh et al., 2018), which would be predicted to preferentially accumulate in deeper-water zones in conjunction with silt- and clay-sized particles. Additionally, the results of multiple linear regression analyses indicated that water depth is a better predictor of As concentrations in near-surface sediments than both Fe and S (Table S11). The occurrence of Type D and Type E profiles in both shallow- and deep-water areas (Fig. 2), however, suggests that water depth is not the only physical control on sediment As concentrations.

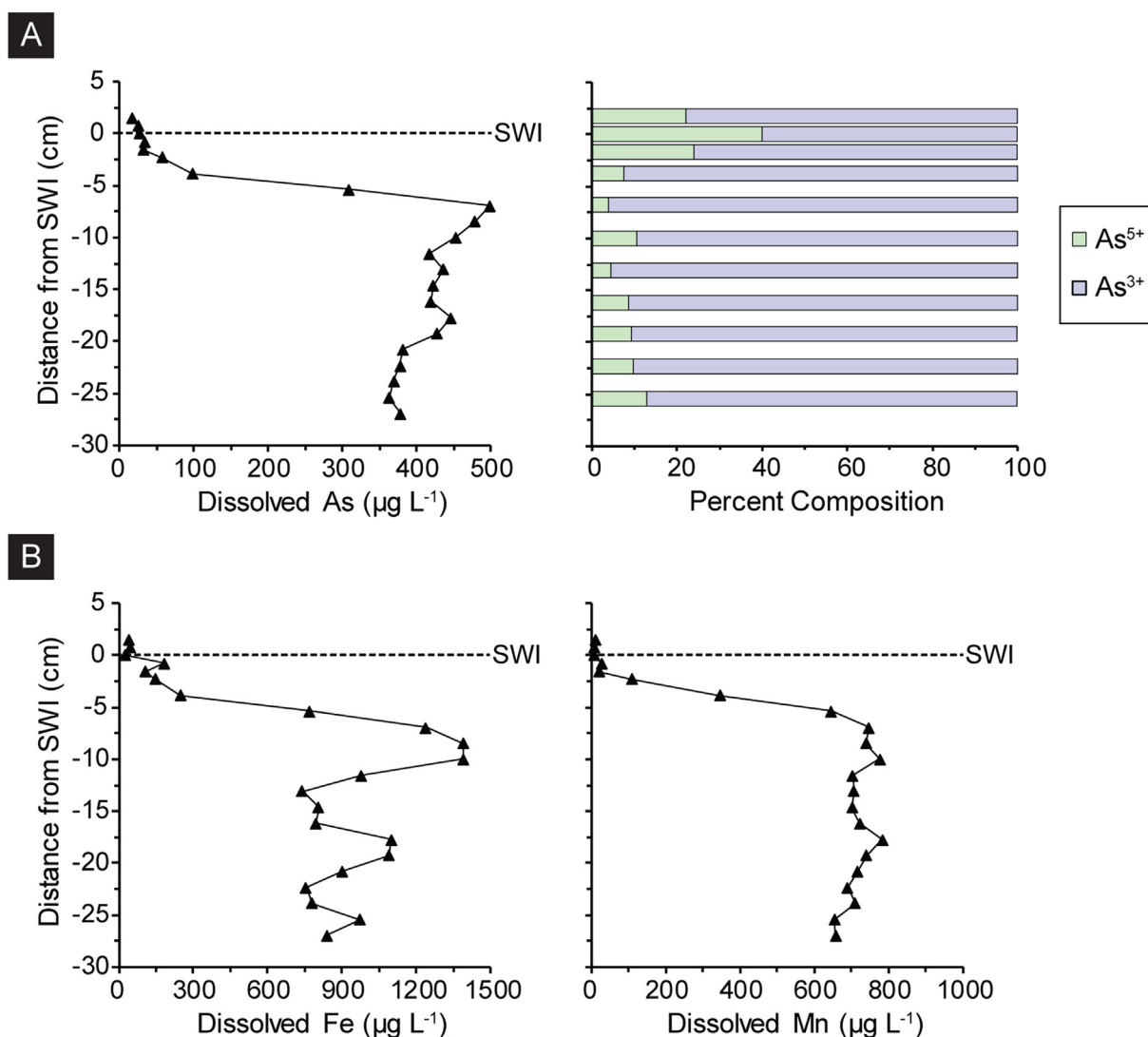


Fig. 5. Concentration profiles of dissolved solutes across the sediment-water interface (SWI) at site LLSP. (a) Dissolved As and corresponding distribution of inorganic As species, and (b) dissolved Fe and Mn. (For interpretation of the references to colour in this figure legend, the reader is referred to the web version of this article.)

Sediment cores collected by Schuh et al. (2018) from relatively deep-water, mid-basin areas in Long Lake (site LLCD) (Fig. 1c) and Martin Lake, which is also located downwind of the former roaster at Giant Mine, featured horizons of maximum As concentration approximately 20 cm below the sediment-water interface, which are characteristic of Type D profiles. Radiometric dating using ²¹⁰Pb revealed that these As-enriched layers, in which virtually 100% of As is hosted in As₂O₃ and authigenic As-bearing sulphides formed from its partial dissolution, correspond to the period of maximum stack emissions (1949–1951) from the Giant Mine roaster (Schuh et al., 2018). Cores collected from depositional zones (Type D), where little to no sediment resuspension is expected to occur, should therefore be enriched in fine-grained particles of As₂O₃ at sediment depths corresponding to the period of maximum stack emissions in the region. Such enrichments are not expected to be present in cores collected from zones of erosion and resuspension, where wave-induced mixing, bioturbation, turbidity currents, gravity-induced slope failures, and ice scouring in winter likely limit the accumulation of fine-grained materials (Blais and Kalff, 1995). Type D sediment As concentration profiles are therefore interpreted to represent areas of sediment deposition and accumulation. Furthermore, the two cores with maximum As concentrations exceeding 3000 mg kg⁻¹, both of which occurred in the 15–20 cm depth interval (cores 37 and

39), were collected from the deep, narrow trench along the northern shore of Long Lake where sediment accumulation rates are likely highest (Fig. 2). High-resolution sediment core LLSP, which was collected in a water depth of 2 m, was enriched in As₂O₃ in sediments 5–6 cm below the sediment-water interface (LLSP-06) (Fig. 3), which indicates that sediments are accumulating at this location, albeit at an inferred lower rate than in deeper areas. This is supported by the As profile and corresponding ²¹⁰Pb-derived timeline in a sediment core collected by Van Den Berghe et al. (2018) from a relatively shallow-water (1 m), nearshore location in Handle Lake, which is also located downwind of the Giant Mine property. In this core, the horizon of peak As concentration occurred at approximately 5 cm depth, contained a high proportion (>90%) of As hosted in As₂O₃ and authigenic sulphides, and was coincident with the onset of ore roasting activities in the area in the 1940s.

In contrast to Type D profiles, the highest sediment As concentrations in Type E profiles occurred at the sediment-water interface and decreased with sediment depth (Fig. 2). This suggests these profiles form in relatively high-energy, erosional environments where sediment accumulation rates are lower. High As concentrations in surficial sediments, relative to deeper layers, may result from the following physical processes, acting alone or in combination: (1) low rates of

sedimentation and burial (i.e., high As concentrations in interfacial sediments correspond to the period of maximum stack emissions), (2) sediment resuspension, mixing, and transport, and (3) continued deposition from terrestrial sources. In Long Lake, these profiles were more commonly found in cores collected from shallow-water areas but were also present in deep-water cores collected on or near to relatively steep basin slopes (Fig. 2). An example is the high-resolution LLDP core, which was collected at 5.5 m water depth and near a slope (Fig. 2) but featured a Type E profile (Fig. 3). The approximately equal proportions of As-bearing Fe-oxyhydroxide (hosting 43% of total As) and realgar (42%) in surficial sediments (LLDP-01), phases that are expected to form in oxidizing and reducing conditions, respectively, suggest that sediments in this core have been physically mixed by slope-related erosional processes or other mixing mechanisms (wind-generated waves, bioturbation, etc.). Therefore, in Long Lake and other lacustrine environments in which the relative timing of As inputs to the sediments can be inferred based on documented emission histories at nearby mines, As concentration profiles in sediment cores and corresponding mass distributions of As-hosting solid phases are useful indicators of lake-wide accumulation trends.

4.2. Geochemical controls on the spatial distribution of arsenic in sediments

In addition to directly influencing the distribution of As in Long Lake sediments by physically redistributing As-bearing particles to areas of deposition, sediment focusing can indirectly affect the distribution of As in sediments by concentrating Fe, S, and OC in the same areas, as these variables were also positively and significantly correlated with water depth in all sediment depth intervals (Fig. 4). The mechanism of co-accumulation for Fe, S, and OC relates to the influence of OC accumulation on redox conditions, sulphate reduction, and the formation of authigenic pyrite (Huerta-Diaz et al., 1998; Couture et al., 2010).

The results of multiple linear regression indicated that Fe concentration is the best predictor of As concentration in Long Lake sediments, as it was only a marginally weaker predictor than water depth in surficial sediments and was the best predictor of As concentration in deeper sediment layers (Table S11). The strong correlation between Fe and As concentration can be explained by the solid-phase association of these two elements in both oxidizing and reducing environments (Martin and Pedersen, 2002; Bostick and Fendorf, 2003; O'Day et al., 2004; Lowers et al., 2007; Andrade et al., 2010; Moriarty et al., 2014; Sprague and Vermaire, 2018; Schuh et al., 2018), though stack emissions from Giant Mine may have also been enriched in Fe (Riveros et al., 2000; Thienpont et al., 2016). In Type D profiles, the partial dissolution of As_2O_3 in deeper sediment horizons creates a concentration gradient that drives the upward diffusion of dissolved As toward the sediment-water interface, resulting in a surficial layer enriched in authigenic As-bearing Fe-oxyhydroxide (Martin and Pedersen, 2002; Andrade et al., 2010; Schuh et al., 2018). Such an enrichment is not evident in the lower-resolution As profiles (Fig. 2), but can be seen in the LLSP profile and the corresponding mass distribution of As-hosting solid phases in sample LLSP-01 (Fig. 3). This highlights the importance of high-resolution sampling in surficial sediments, as it is possible that cores classified as Type E might actually represent Type D cores with very shallow As peaks. Nevertheless, As enrichments at depth in the sediment column were notably absent in Type E profiles. However, particles of As-bearing Fe-oxyhydroxide may be supplied to the sediment surface as part of the accumulating material before they are ultimately redistributed to areas of sediment deposition elsewhere in the lake basin (Boudreau, 1999). It is also possible that during the period of maximum regional emissions, the rate at which As_2O_3 was deposited and buried in areas characterized by Type E profiles was exceeded by the rate at which As_2O_3 dissolved and released As to sediment porewaters. The resulting concentration gradient would drive upward diffusion and result in surficial sediments being enriched in As (hosted in Fe-oxyhydroxide) relative to deeper layers.

At greater sediment depths, Fe was the strongest predictor of sediment As concentration (Table S11) because of the association between As and framboidal pyrite, and the co-accumulation of discrete As-sulphides (i.e., realgar) in the same horizons as authigenic pyrite. The progressive burial of sediments over time leads to the development of reducing conditions, and particles of As-bearing Fe-oxyhydroxide reductively dissolve and release ferrous Fe (Fe^{2+}) and As to porewaters. Aqueous reduced S (S^{2-}) first reacts with Fe^{2+} to form framboidal pyrite (Morse and Rickard, 2004), which may sequester dissolved As through adsorption or co-precipitation. Only after Fe^{2+} has been removed from solution through pyrite formation will S^{2-} remaining in solution become available to react with As to form realgar (Wilkin and Ford, 2003; Wilkin et al., 2006), due to its higher solubility in comparison to pyrite (O'Day et al., 2004). Iron was therefore a better predictor of sediment As concentration than S in all depth intervals, even in sediments >5 cm below the sediment surface, which contained abundant realgar formed in situ from the partial dissolution of As_2O_3 . Framboidal pyrite was the predominant host of As in depth intervals where As concentrations are assumed to represent pre-mining levels (samples LLSP-24 and LLDP-25), which occurred at 10–20 cm depth in both high-resolution cores (Fig. 3). The regression coefficient for S within the 15–20 cm depth interval in survey cores was negative (Table S11), indicating that an increase in S concentration is associated with a decrease in As concentration. This suggests that framboidal pyrite is the principal host of As at this depth and that As is substituting for S in the crystal structure of pyrite, which has been documented previously in Long Lake sediments and in other environments (Savage et al., 2000; Lowers et al., 2007; Schuh et al., 2018).

4.3. Spatial heterogeneity of arsenic fluxes

The calculated rates of As remobilization and efflux across the benthic boundary (Table S13) indicate that As in sediments is upwardly mobile and sediments are a source of dissolved As to surface waters. These results are consistent with previous studies that calculated As fluxes from contaminated sediments in the Yellowknife area (Andrade et al., 2010; Van Den Berghe et al., 2018). Inherent in these calculations were several assumptions: (1) that the dissolved As concentration gradients measured across the sediment-water interface at sites LLSP and LLPC (Schuh et al., 2018) (Fig. 1c) are linear, (2) that other transportation mechanisms that may influence rates of As diffusion (bioturbation, physical mixing of sediments, etc.) can be ignored, and (3) that sediment porosity and tortuosity can be estimated a priori based on grain size. Furthermore, these calculations were based on single time point measurements of the dissolved As concentration gradients at both sites, which are likely to exhibit seasonal variation (Martin and Pedersen, 2002; Andrade et al., 2010).

Calculated rates of upward As remobilization for both As^{5+} and As^{3+} were considerably greater at site LLSP than at site LLPC (Schuh et al., 2018) (Table S13). Similarly, calculated rates of diffusion across the sediment-water interface for both aqueous inorganic As species were approximately two times greater at LLSP than at LLPC (Table S13). These sites are both located in relatively shallow water (2 m and 0.7 m water depths for LLSP and LLPC, respectively) (Fig. 1c), which suggests that the magnitude of porewater concentration gradients can exhibit substantial spatial variation due to slight changes in sediment texture, solid-phase chemical composition, and sediment porosity, which are in turn caused by changes in water depth and textural sorting. Comparatively, both the low and high estimates of As burial rate exceed rates of As diffusion by 1–2 orders of magnitude, suggesting that rates of As_2O_3 dissolution and release into the overlying water column, at least during the period of maximum stack emissions in the region, did not “keep pace” with the rate at which aerially deposited As was buried in sediments. This may explain why Type D profiles, which are interpreted to represent depositional zones, closely resemble historical emission patterns. However, these estimates assume that the sedimentation

rate measured in a relatively deep-water, depositional environment (site LLCD) (Schuh et al., 2018) (Fig. 1c) can be extrapolated to site LLSP where deposition rates are inferred to be lower, and that sedimentation rates have remained relatively constant over time.

Sediment-focusing processes may also indirectly influence dissolved As fluxes by altering redox conditions within the sediment column. At site LLSP, the concavity of the porewater profile of dissolved As (Fig. 5a) and predominance of As-bearing Fe-oxyhydroxide (Fig. 3) in near-surface sediments indicates that a portion of the upward-diffusing As is sequestered in the interfacial sediments before reaching the water column. During ice-free periods, this profile can be assumed to be in pseudo-steady-state, whereby the inventory of available Fe-oxyhydroxide in the surface layer is sustained through the continued reductive dissolution of Fe-oxyhydroxides at depth (through progressive burial), upward diffusion of Fe^{2+} , and re-precipitation in oxic horizons (Davison, 1993). Higher accumulation rates of OC in surficial sediments, however, will increase oxidation rates, decrease the thickness of the oxic surface layer, and enhance rates of diffusion into the overlying water column (Martin and Pedersen, 2002). Therefore, rates of remobilization and efflux are higher at LLSP where the oxic surface horizon is inferred to be thinner than at LLPC based on the shallower depth of the porewater maximum and greater magnitude of the concentration gradient. Diffusion rates of As are also dependent on aqueous speciation, as the diffusion coefficient for As^{3+} is higher than that for As^{5+} (Table S13). The high relative proportion of As^{3+} in both bottom waters and near-surface porewaters at site LLSP (Fig. 5; Table S12) suggests that As^{5+} is preferentially removed by authigenic Fe-oxyhydroxide, which has been documented in laboratory studies (Dixit and Hering, 2003), and that As^{3+} is more mobile across the sediment-water interface. Thus, rates of As diffusion into surface waters are enhanced at LLSP relative to LLPC, where As^{5+} is the predominant aqueous species in porewaters below the sediment-water interface (Schuh et al., 2018). Based on the results from these two sites, it is likely that in deep-water zones of deposition where TOC concentrations in surficial sediments are highest (Table S7) and $\text{As}^{5+}/\text{As}^{3+}$ ratios are presumably low, rates of As release into the water column are even higher.

4.4. Implications for risk assessment

The spatial heterogeneity of sediment As concentrations, solid-phase speciation, and diffusive fluxes observed in this study has implications for human health and ecological risk assessments in the Yellowknife area and in other aquatic environments affected by the atmospheric deposition of As. The interim sediment quality guideline (ISQG) and probable effect level (PEL) outlined by the Canadian Council of Ministers of the Environment (CCME) are dry-weight concentration benchmarks used to determine the likelihood of adverse biological effects occurring as a result of exposure to solid-phase As in surficial sediments (i.e., top 5 cm) (CCME, 1999). For As, the ISQG is 5.9 mg kg^{-1} and the PEL is 17 mg kg^{-1} (CCME, 1999). In Long Lake, 96% ($n = 45$) of measured As concentrations in near-surface sediments exceeded the PEL. Arsenic concentrations in this depth interval, however, were positively and significantly correlated ($\rho = 0.86$, $p < 0.001$) with water depth (Fig. 4). Moreover, the highest As concentrations (Fig. 2; Table S2) occurred in deep-water areas where human exposure to sediments is unlikely. In contrast, surficial sediment As concentrations in the beach and boat launch area (Fig. 2; Table S2), which was previously targeted as part of the recent HHRA (Canada North Environmental Services, 2018), were among the lowest observed in this study.

The potential for deleterious effects to occur in humans from exposure to sediment-bound As is known to be largely dependent on bioaccessibility, which in turn depends on solid-phase speciation. More than 60 years after the period of maximum stack emissions in the region, highly bioaccessible As_2O_3 (Plumlee and Morman, 2011) has persisted

in high concentrations in Long Lake sediments (Fig. 3), but mostly in deep-water areas where the potential for direct human exposure is low. The partial dissolution of As_2O_3 and subsequent formation of secondary As-hosting phases including realgar, arsenian pyrite, and As-bearing Fe-oxyhydroxide also represents an effective “natural” mechanism for reducing As bioaccessibility as these phases are all less bioaccessible than As_2O_3 (Plumlee and Morman, 2011).

Despite the formation of secondary As-hosting phases that reduce the bioaccessibility and mobility of As in solid form, sediments in Long Lake are an ongoing source of dissolved As to the overlying water column. Rates of As diffusion across the sediment-water interface are inferred to be spatially variable due to differences in sediment texture and composition, and are likely higher in deep-water, depositional zones. Recent work by Barrett et al. (2018) has shown that the mobilization of As from contaminated sediments into small, shallow lakes with well-mixed water columns, such as Long Lake during summer, increases As uptake by aquatic organisms that occupy lower trophic levels, which may influence the bioaccumulation and trophic transfer of As.

5. Conclusions

Arsenic concentrations and solid-phase speciation in Long Lake sediments exhibited considerable lateral and vertical variation, which can be attributed to physical processes that redistribute As and other elements involved in its redox cycling from zones of sediment erosion to areas of sediment deposition. These zones can be distinguished using down-core As concentration profiles and their corresponding mass distributions of As-hosting solid phases. Water depth, as a proxy for sediment focusing, is the best predictor of As concentrations in near-surface sediments, but is a weaker predictor of As concentrations in deeper sediment layers due to the existence of the two types of As profile identified in this study. Iron concentration, as an indicator of As, Fe, and S co-diagenesis, and possibly co-occurrence in stack emissions, is a better predictor of As concentration at greater sediment depths. Calculated rates of dissolved As remobilization and diffusion-controlled release to bottom water at two sites suggests that dissolved As fluxes are spatially variable as a result of sediment redistribution and its influence on redox conditions within the sediment column.

The spatial heterogeneity of As distribution observed in this study emphasizes the advantages of a multi-station approach for capturing whole-lake accumulation trends. Furthermore, an understanding of the depositional patterns of atmospherically deposited As in sediments is important in the context of risk assessment, as it highlights areas of lakes where exposure to high sediment As concentrations, more bioaccessible As-hosting solid phases, and enhanced rates of As release to the water column are most likely. Future work should aim to quantify the effects of sediment focusing, possibly through the radiometric dating of multiple cores, to better elucidate the influence of textural sorting on the long-term fate of As in mine-impacted lakes.

Acknowledgments

This study was partially funded by a Natural Sciences and Engineering Research Council of Canada (NSERC) Strategic Grant (Grant #309983638) awarded to Jules Blais (Principal Investigator), and H. E. Jamieson, John Smol, and Alexandre Poulain (co-Principal Investigators), and by the Government of the Northwest Territories Cumulative Impact Monitoring Program (GNWTCIMP, Project #168). The authors would also like to thank Agatha Dobosz, Jon Oliver, and Ryan Shaw of Queen's University, the Analytical Services Unit (ASU) at Queen's University, Judy Mah and Taiga Environmental Laboratory, Dominic Bélanger of Université de Montréal, and Shawne Kokelj and Robin Staples from GNWT-Water Resources.

Appendix A. Supplementary data

Supplementary data to this article can be found online at <https://doi.org/10.1016/j.scitotenv.2018.11.065>.

References

- Andrade, C.F., Jamieson, H.E., Kyser, T.K., Praharaj, T., Fortin, D., 2010. Biogeochemical redox cycling of arsenic in mine-impacted lake sediments and co-existing pore waters near Giant Mine, Yellowknife Bay, Canada. *Appl. Geochem.* 25, 199–211.
- Appleby, P.G., 2001. Chronostratigraphic techniques in recent sediments. In: Last, W.M., Smol, J.P. (Eds.), *Tracking Environmental Change, and Chronological Techniques*. Kluwer Academic Publishers, Dordrecht, The Netherlands, pp. 171–204.
- Barrett, P.M., Hull, E.A., King, C.E., Burkart, K., Ott, K.A., Ryan, J.N., Gawel, J.E., Neumann, R.B., 2018. Increased exposure of plankton to arsenic in contaminated weakly-stratified lakes. *Sci. Total Environ.* 625, 1606–1614.
- Bednar, A.J., Garbarino, J.R., Ranville, J.F., Wildeman, T.R., 2002. Preserving the distribution of inorganic arsenic species in groundwater and acid mine drainage samples. *Environ. Sci. Technol.* 36, 2213–2218.
- Bissen, M., Frimmel, F.H., 2003. Arsenic – a review. Part I: occurrence, toxicity, speciation, mobility. *Acta Hydrochim. Hydrobiol.* 31, 9–18.
- Blais, J.M., Kalff, J., 1995. The influence of lake morphometry on sediment focusing. *Limnol. Oceanogr.* 40, 582–588.
- Bostick, B.C., Fendorf, S., 2003. Arsenite sorption on troilite (FeS) and pyrite (FeS₂). *Geochim. Cosmochim. Acta* 67, 909–921.
- Boudreau, B.P., 1999. Metals and models: diagenetic modelling in freshwater lacustrine sediments. *J. Paleolimnol.* 22, 227–251.
- Bowell, R.J., Alpers, C.N., Jamieson, H.E., Nordstrom, D.K., Majzlan, J., 2014. The environmental geochemistry of arsenic – an overview. *Rev. Mineral. Geochem.* 79, 1–16.
- Campbell, K.M., Root, R., O'Day, P.A., Hering, J.G., 2008. A gel probe equilibrium sampler for measuring arsenic porewater profiles and sorption gradients in sediments: II. Field application to Haiwee Reservoir sediment. *Environ. Sci. Technol.* 42, 504–510.
- Canada North Environmental Services, 2018. Giant Mine Human Health and Ecological Risk Assessment. Project No. 2385. Prepared for Public Services and Procurement Canada (305 pages).
- Canadian Council of Ministers of the Environment, 1999. Canadian sediment quality guidelines for the protection of aquatic life: Arsenic. Canadian Environmental Quality Guidelines. Canadian Council of Ministers of the Environment, Winnipeg, MB <http://ceqg-rceq.cme.ca/download/en/230/>, Accessed date: 15 October 2018.
- Carter, M.R., Gregorich, E.G., 2007. *Soil Sampling and Methods of Analysis*, second ed. Taylor & Francis Group, Boca Raton, FL.
- Couture, R.-M., Gobeil, C., Tessier, A., 2010. Arsenic, iron, and sulfur co-diagenesis in lake sediments. *Geochim. Cosmochim. Acta* 74, 1238–1255.
- Craw, D., Bowell, R.J., 2014. The characterization of arsenic in mine waste. *Rev. Mineral. Geochem.* 79, 473–505.
- Creed, J.T., Brockhoff, C.A., Martin, T.D., 1994. Method 200.8, Revision 5.4: Determination of Metals and Trace Elements in Water and Wastes by Inductively Coupled Plasma-mass Spectrometry. United States Environmental Protection Agency, Cincinnati, OH https://www.epa.gov/sites/production/files/2015-08/documents/method_200-8_rev_5-4_1994.pdf, Accessed date: 30 April 2018.
- Davison, W., 1993. Iron and manganese in lakes. *Earth-Sci. Rev.* 34, 119–163.
- Dixit, S., Hering, J.G., 2003. Comparison of arsenic(V) and arsenic(III) sorption onto iron oxide minerals: implications for arsenic mobility. *Environ. Sci. Technol.* 37, 4182–4189.
- Engstrom, D.R., Rose, N.L., 2013. A whole-basin, mass-balance approach to paleolimnology. *J. Paleolimnol.* 49 (3), 333–347.
- Environment Canada, 2017. Canadian climate normals 1971–2000 station data: Yellowknife Airport. http://climate.weather.gc.ca/climate_normals/results_e.html?stmlID=1706, Accessed date: 25 July 2017.
- Galloway, J.M., Palmer, M.J., Jamieson, H.E., Patterson, R.T., Nasser, N., Falck, H., Macumber, A.L., Goldsmith, S.A., Sanei, H., Roe, H.M., Neville, L.A., Lemay, D., 2015. Geochemistry of lakes across ecozones in the Northwest Territories and implications for the distribution of arsenic in the Yellowknife region. Part 1: sediments. Geological Survey of Canada, Open File 7908, p. 1.
- Galloway, J.M., Swindles, G.T., Jamieson, H.J., Palmer, M., Parsons, M.B., Sanei, H., Macumber, A.L., Patterson, R.T., Falck, H., 2018. Organic matter control on the distribution of arsenic in lake sediments impacted by ~65 years of gold ore processing in subarctic Canada. *Sci. Total Environ.* 622–623, 1668–1679.
- Glew, J., 1989. A new trigger mechanism for sediment core sampling. *J. Paleolimnol.* 2, 241–243.
- Groves, D.J., Goldfarb, R.J., Gebre-Mariam, M., Hagemann, S.G., Robert, F., 1998. Orogenic gold deposits: a proposed classification in the context of their crustal distribution and relationship to other gold deposit types. *Ore Geol. Rev.* 13, 7–27.
- Håkanson, L., 1977. The influence of wind, fetch, and water depth on the distribution of sediments in Lake Vänern, Sweden. *Can. J. Earth Sci.* 14, 397–412.
- Håkanson, L., Jansson, M., 2011. *Principles of Lake Sedimentology*. Springer-Verlag, Berlin.
- Hamilton, D.P., Mitchell, S.F., 1997. Wave-induced shear stresses, plant nutrients and chlorophyll in seven shallow lakes. *Freshw. Biol.* 38, 159–168.
- Harris, R., Jarvis, C., 2010. *Statistics for Geography and Environmental Science*. first ed. Routledge, London.
- Health Canada, 2010. Federal contaminated site risk assessment in Canada, Part V: Guidance on human health detailed quantitative risk assessment for chemicals (DQRChem). Prepared by Contaminated Sites Division Safe Environments Directorate (112 pages). http://publications.gc.ca/collections/collection_2011/sc-hc/H128-1-11-639-eng.pdf, Accessed date: 17 October 2018.
- Héquette, A., Tremblay, P., Hill, P.R., 1999. Nearshore erosion by combined ice scouring and near-bottom currents in eastern Hudson Bay, Canada. *Mar. Geol.* 158, 253–266.
- Huerta-Diaz, M.A., Tessier, A., Carnigan, R., 1998. Geochemistry of trace metals associated with reduced sulfur in freshwater sediments. *Appl. Geochem.* 13, 213–233.
- Lin, Q., Liu, E., Zhang, E., Nath, B., Shen, J., Yuan, H., Wang, R., 2018. Reconstruction of atmospheric trace metals pollution in Southwest China using sediments from a large and deep alpine lake: historical trends, sources and sediment focusing. *Sci. Total Environ.* 613, 331–341.
- Lowers, H.A., Breit, G.N., Foster, A.L., Whitney, J., Yount, J., Uddin, Md.N., Muneem, Ad.A., 2007. Arsenic incorporation into authigenic pyrite, Bengal Basin sediment, Bangladesh. *Geochim. Cosmochim. Acta* 71, 2699–2717.
- Mackay, E.B., Jones, I.D., Folkard, A.M., Barker, P., 2012. Contribution of sediment focussing to heterogeneity of organic carbon and phosphorus burial in small lakes. *Freshw. Biol.* 57, 290–304.
- Mackenzie Valley Review Board, 2013. Report of Environmental Assessment and Reasons for Decision, Giant Mine Remediation Project. EA0809-001. http://reviewboard.ca/upload/project_document/EA0809-001_Giant_Report_of_Environmental_Assessment_June_20_2013.PDF, Accessed date: 18 October 2017.
- Manger, G.E., 1963. Porosity and bulk density of sedimentary rocks. United States Geological Survey Bulletin 1144-E <https://pubs.usgs.gov/bul/1144e/report.pdf>, Accessed date: 27 January 2018.
- Marsden, J.O., House, C.I., 2006. *The Chemistry of Gold Extraction*. Society for Mining, Metallurgy, and Exploration, Inc. U.S.A.
- Martin, A.J., Pedersen, T.F., 2002. Seasonal and interannual mobility of arsenic in a lake impacted by metal mining. *Environ. Sci. Technol.* 36, 1516–1523.
- Martin, T.D., Creed, J.T., Brockhoff, C.A., 1994a. USEPA Method 200.2, Revision 2.8: Sample preparation procedure for spectrochemical determination of total recoverable elements. https://www.epa.gov/sites/production/files/2015-08/documents/method_200-2_rev_2-8_1994.pdf, Accessed date: 30 April 2018.
- Martin, T.D., Brockhoff, C.A., Creed, J.T., 1994b. USEPA Method 200.7, Revision 4.4: Determination of metals and trace elements in water and wastes by inductively coupled plasma-atomic emission spectrometry. https://www.epa.gov/sites/production/files/2015-08/documents/method_200-7_rev_4-4_1994.pdf, Accessed date: 30 April 2018.
- Moriarty, M.M., Lai, V.W.-M., Koch, I., Cui, L., Combs, C., Krupp, E.M., Feldmann, J., Cullen, W.R., Reimer, K.J., 2014. Speciation and toxicity of arsenic in mining-affected lake sediments in the Quinsam watershed, British Columbia. *Sci. Total Environ.* 466–467, 90–99.
- Morse, J.W., Rickard, D., 2004. Chemical dynamics of sedimentary acid volatile sulfide. *Environ. Sci. Technol.* 38, 131A–136A.
- O'Brien, R.M., 2007. A caution regarding rules of thumb for variance inflation factors. *Qual. Quant.* 41, 673–690.
- O'Day, P.A., Vlassopoulos, D., Root, R., Rivera, N., 2004. The influence of sulfur and iron on dissolved arsenic concentrations in the shallow subsurface under changing redox conditions. *Proc. Natl. Acad. Sci. U. S. A.* 101, 13703–13708.
- Palmer, M.J., Galloway, J.M., Jamieson, H.E., Patterson, R.T., Falck, H., Kokelj, S.V., 2015. The concentration of arsenic in lake waters of the Yellowknife area. Northwest Territories Geological Survey, NWT Open File 2015-06 (25 p).
- Plumlee, G.S., Morman, S.A., 2011. Mine wastes and human health. *Elements* 7, 399–404.
- Rippey, B.R., Anderson, N.J., Renberg, I., Korsman, T., 2008. The accuracy of methods used to estimate the whole-lake accumulation rate of organic carbon, major cations, phosphorus and heavy metals in sediment. *J. Paleolimnol.* 39, 83–99.
- Riveros, P.A., Dutrizac, J.E., Chen, T.T., 2000. Recovery of marketable arsenic trioxide from arsenic-rich roaster dust. In: Sánchez, M.A., Vergara, F., Castro, S.H. (Eds.), *Fifth International Conference on Clean Technologies for the Mining Industry*. vol. II. University of Concepción, Concepción, Chile, pp. 135–149.
- Savage, K.S., Tingle, T.N., O'Day, P.A., Waychunas, G.A., Bird, D.K., 2000. Arsenic speciation in pyrite and secondary weathering phases, Mother Lode gold district, Tuolumne county, California. *Appl. Geochem.* 15, 1219–1244.
- Schuh, C.E., Jamieson, H.E., Palmer, M.J., Martin, A.J., 2018. Solid-phase speciation and post-depositional mobility of arsenic in lake sediments impacted by ore roasting at legacy gold mines in the Yellowknife area, Northwest Territories, Canada. *Appl. Geochem.* 91, 208–220.
- Shepard, F.P., 1954. Nomenclature based on sand-silt-clay ratios. *J. Sediment. Petrol.* 24, 151–158.
- Smedley, P.L., Kinniburgh, D.G., 2002. A review of the source, behaviour and distribution of arsenic in natural waters. *Appl. Geochem.* 17, 517–568.
- Sprague, D.D., Vermaire, J.C., 2018. Legacy arsenic pollution of lakes near Cobalt, Ontario, Canada: arsenic in lake water and sediment remains elevated nearly a century after mining activity has ceased. *Water Air Soil Pollut.* 229, 87. <https://doi.org/10.1007/s11270-018-3741-1>.
- Tanaka, M., Takahashi, Y., Yamaguchi, N., Kim, K.-W., Zheng, G., Sakamitsu, M., 2013. The difference of diffusion coefficients in water for arsenic compounds at various pH and its dominant factors implied by molecular simulations. *Geochim. Cosmochim. Acta* 105, 360–371.
- Thienpont, J.R., Korosi, J.B., Hargan, K.E., Williams, T., Eickmeyer, D.C., Kimpe, L.E., Palmer, M.J., Smol, J.P., Blais, J.M., 2016. Multi-trophic level response to extreme metal contamination from gold mining in a subarctic lake. *Proc. R. Soc. B* 283, 20161125. <https://doi.org/10.1098/rspb.2016.1125>.
- Ullman, W.J., Aller, R.C., 1982. Diffusion coefficients in nearshore marine sediments. *Limnol. Oceanogr.* 27, 552–556.

- Van Den Berghe, M.D., Jamieson, H.E., Palmer, M.J., 2018. Arsenic mobility and characterization in lakes impacted by gold ore roasting, Yellowknife, NWT, Canada. *Environ. Pollut.* 234, 630–641.
- Walker, S.R., Jamieson, H.E., Lanzirotti, A., Hall, G.E.M., Peterson, R.C., 2015. The effect of ore roasting on arsenic oxidation state and solid phase speciation in gold mine tailings. *Geochem. Explor. Environ. Anal.* 15, 273–291.
- Wilkin, R.T., Ford, R.G., 2003. Speciation of arsenic in sulfidic waters. *Geochem. Trans.* 4, 1–7.
- Wilkin, R.T., Wallschläger, D., Ford, R.G., 2006. Arsenic solid-phase partitioning in reducing sediments of a contaminated wetland. *Chem. Geol.* 228, 156–174.
- Wrye, L.A., 2008. Distinguishing Between Natural and Anthropogenic Sources of Arsenic in Soils From the Giant Mine, Northwest Territories, and the North Brookfield Mine, Nova Scotia. (M.Sc. Thesis). Queen's University.